Exp Fluids
DOI 10.1007/s00348-011-1047-9

RESEARCH ARTICLE

Modeling of dual emission laser induced fluorescence for slurry thickness measurements in chemical mechanical polishing

Caprice Gray · Chris B. Rogers · Vincent P. Manno · Robert D. White

Received: 31 July 2010 / Revised: 27 December 2010 / Accepted: 27 January 2011

Abstract Dual emission laser induced fluorescence (DELIF) is a technique for measuring the instantaneous thin fluid film thickness in dynamic systems. Two fluorophores within the system produce laser induced emissions that are filtered and captured by two cameras. The ratio of the images from these cameras is used to cancel the effect of the laser beam profile on the image intensity. The resultant intensity ratio can be calibrated to a fluid film thickness. The utilization of a 2-dye system when applied to Chemical Mechanical Polishing (CMP) is complicated by the fluorescence of the polymeric polishing pad and the light scattering particles in the polishing slurry. We have developed a model of DELIF for CMP with 1-dye employing the polishing pad as the second fluorophore. While scattering particles in the slurry decrease the overall intensity of the individual images, the contrast in the image ratio increases. Using the 1-dye DELIF system to measure thin slurry films, our model results indicate that a cubic calibration may be needed. However, experimental results suggest a linear calibration is achieved for slurry films between 0 and 133 μm thick with scattering coefficients as high as 8.66 mm^{-1} at a wavelength equal to 410 nm.

1 Introduction: dual emission laser induced fluorescence

Dual emission laser induced fluorescence (DELIF) has historically been used to acquire instantaneous, in situ measurements for a variety of "passive scalar" quantities in thin fluid films as discussed by Coppeta and Rogers (1998). Some of the most common applications of DELIF include solute concentrations and flow field measurements (Shlien 1998; Arcoumanis et al. 1990; Strömberg and Hulth 2005), pH measurements (Coppeta and Rogers 1998; Bassnett et al. 1990), and temperature field measurements (Sakakibara and Adrian 1999, 2004). An extensive model of this system was developed by Hidrovo and Hart (2001) and was finally experimentally applied to CMP in 2003 by Chan and Rogers (2003).

Historically, DELIF had been performed using two dyes dissolved in a thin fluid film (Coppeta and Rogers 1998; Hidrovo and Hart 2001; Chan 2003). In CMP, this fluid film exists between the substrate and substrate chuck that is being polished and the polishing pad. In the Hidrovo and Hart experiments, the fluid film existed between a glass slide and a US quarter (Hidrovo and Hart 2001). A schematic of the cross section of this system is shown in Fig. 1. This system was shown to measure fluid layer thickness over substrates with roughness on the order of tens of microns (Hidrovo and Hart 2001; Chan 2003; Lu et al. 2000).

The DELIF technique for measure thin fluid film thickness uses the ratio of two different emissions produced by dyes dissolved in the fluid layer (Coppeta and Rogers 1998; Hidrovo and Hart 2001). These emissions are filtered and collected into two CCD cameras. This system requires a high-energy fluorophore that is capable of absorbing at the wavelength of the laser emission and lower energy fluorophore that absorbs the emission of the high-energy fluorophore and, in turn, emits at lower energy. Both emissions exit the thin fluid film and travel toward a lens that collects emissions across the full visual spectrum. The fluorescent light is filtered such that one camera collects the high-energy emission, and a second camera collects the lower energy emission. A more detailed description of

C. Gray (✉) · C. B. Rogers · V. P. Manno · R. D. White
Tufts University, Medford, MA 02155, USA
e-mail: cappy@alum.mit.edu

Published online: 15 February 2011

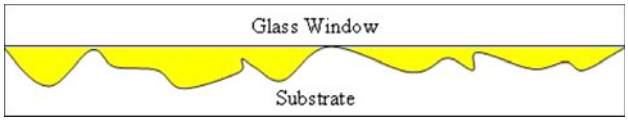

Fig. 1 A diagram of the Hidrovo and Hart (2001) DELIF system for measuring the thickness of thin fluid films

the experimental setup is briefly described later and can be found in previous work (Hidrovo and Hart 2001; Chan 2003; Lu et al. 2000; Rogers et al. 1998; Coppeta et al. 2000; Apone et al. 2005).

The final ratiometric image of the emission from dye 1 to emission of dye 2 was shown to correlate linearly with fluid film thickness for thin fluid films (Coppeta and Rogers 1998; Hidrovo and Hart 2001) over thickness variations on the order of 100 microns (Chan 2003; Lu et al. 2000; Rogers et al. 1998). Coppeta and Rogers showed that the measured DELIF ratio, R, for a 2-dye system is:

$$R = \frac{I_{f1}}{I_{f2}} = \frac{\varepsilon_1(t,\lambda)C_1\phi_1}{\varepsilon_2(\lambda)C_2\phi_2} \tag{1}$$

where t is the fluid layer thickness, λ is the wavelength of the excitation source, I_{f1} and I_{f2} are the fluorescent intensities of the thickness-dependent and thickness-independent dyes, ε_1 and ε_2 are the absorption coefficients, C_1 and C_2 are the dye concentrations, and ϕ_1 and ϕ_2 are the dye emission efficiencies (Coppeta and Rogers 1998). Equation 1 is based on the linear form of Beer's Law (McQuarrie and Simon 1997) for a single beam of light passing through a fluid in one direction. I_{f1} is thickness dependent because its emission is reabsorbed by the dye producing I_{f2}. When the fluid layer is thick, more reabsorption occurs producing a weaker I_{f1} signal. Hidrovo and Hart proved that some DELIF systems have inherent nonlinearities in the calibration of intensity to thickness if the incident photon flux is too high (Hidrovo et al. 2004). The excited state of the dye molecules become saturated leading to a nonlinear dependence of the dye on excitation intensity (Hidrovo et al. 2004). In the work presented here, we assume that photon flux of the incident laser on the fluid film is not high enough to produce nonlinearities.

The techniques outlined to model DELIF by Hidrovo and Hart (2001) were not directly transferable to CMP. Additionally, the DELIF model for CMP developed by Coppeta and Rogers (1998) was based on assumptions that are not necessarily practical experimentally. The polishing pad in CMP is often made of polyurethane (Gray 2008) that has a fluorescent emission under ultraviolet light (Chan 2003; Coppeta et al. 1996). This fluorescence changes the boundary condition in the model and can interfere with the other fluorescent signals in the system. When DELIF was applied experimentally, it was necessary to impregnate the polyurethane with a strong absorber, such as carbon black, to suppress the fluorescence (Chan 2003; Lu et al. 2000; Coppeta et al. 2000; Li et al. 2006). Suppression of the polyurethane emission is an imperfect strategy. In previous work, we found that a carbon black infused surface only suppressed the pad emission by a little more than 50% (Gray 2005). Another difference between the system we model here and previously modeled systems is that we account for light scattering with the fluid film. Scattering can occur in any colloidal fluid. CMP slurries are often colloidal particles (Cook 1990) that scatter light, which had not been considered in prior DELIF models.

In this paper, we present a DELIF model for CMP and illustrate how to extract fluid height profiles from this system. To simplify the optical system, we decided to take advantage of the polishing pad fluorescence instead of trying to suppress it (Gray et al. 2005). We have eliminated the use of the high-energy emission dye and have substituted the pad fluorescence in its place. The 1-dye DELIF optical system that we report herein is a significant departure from the Hidrovo and Hart and Coppeta and Rogers models. The Hidrovo and Hart DELIF experiments used a clear oil film (Hidrovo and Hart 2001), and Coppeta and Rogers assumed that scattering effects were insignificant (Coppeta and Rogers 1998). Besides the different geometric location of the fluorophores, previous DELIF models do not account for light scattering in the fluid. In CMP, the fluid layer often contains high concentrations of silica, alumina, or ceria nanoparticles, which are believed to be primarily responsible for material removal (Cook 1990). For in situ CMP measurements, the following model and discussion will consider the effects of light scattering due to the slurry particles and accounts for the single-dye/polyurethane fluorophore geometry that was not considered in previous literature. A list of variables, their units and their physical meaning is provided for the reader in Table 1.

2 Model

Figure 2 illustrates a one-dimensional (x) model of a column of fluid in the 2-dye DELIF system that has been used by both Coppeta and Rogers (1998) and Hidrovo and Hart (2001). Dye 1 is the thickness-dependent dye, represented by the blue dots in Fig. 2. Dye 2 is the thickness-independent dye, represented by the green dots in Fig. 2. The variable, L, is the fluid layer thickness at a single location within the area of interrogation. The laser excitation, I_e, enters the column of fluid at $x = 0$ and travels in the $+x$ direction. As the laser light travels through the column of fluid, both dyes fluoresce. Dye 1 fluoresces in the high-energy portion of the visible spectrum (violet-blue), and Dye 2 fluoresces at a lower energy (green). Dye 2 receives additional excitation from Dye 1 because the absorption

Table 1 List of variables, units, and physical meanings used in the simplified radiative transfer model for the DELIF system

Variable	SI units	Meaning	Subscripts and superscripts
R	Unitless	Ratio of fluorophore 1 intensity to fluorophore 2 intensity	
I	W	Fluorophores 1 and 2 intensity (radiant flux) in 1 camera pixel	$f1$ = fluorophore 1, $f2$ = fluorophore 2, p = pad, d = dye, $+$ = $+x$ direction, $-$ = $-x$ direction
ε	L mol^{-1} m^{-1}	Molar absorptivity	1 = fluorophore 1, 2 = fluorophore 2
C	mol L^{-1}	Concentration	1 = fluorophore 1, 2 = fluorophore 2, d = dye, Si = slurry particles
ϕ	Unitless	Emission efficiency (number of photons emitted)/(number of photons absorbed) for fluorophores 1 and 2	1 = fluorophore 1, 2 = fluorophore
λ	m	Wavelength	l = laser, p = pad
x	m	Axis along which light is propagating	
L	m	Total thickness of the fluid layer	
σ_{em}	W	Intensity of light generated in the fluid layer due to the fluorescents of the fluorophores in the system	
σ_{ext}	Unitless	Extinction coefficient containing unitless scattering and absorption terms that decrease the intensity of the overall system	
μ	L mol^{-1} m^{-1}	Scattering coefficients	f = forward, b = backward
k_1	m^{-1}	Constant representing dye absorption at the wavelength of the laser emission	
k_2	m^{-1}	Constant representing dye absorption at the wavelengths of the pad emission	
k_3	m^{-1}	Constant representing particle scattering	
k_4	Unitless	Constant representing the fluorescent emission of the dye	
k_5	Unitless	Constant representing the fluorescent emission of the pad	
ρ	Unitless	Constant representing the fraction of light reflected off the boundary at $x = L$	

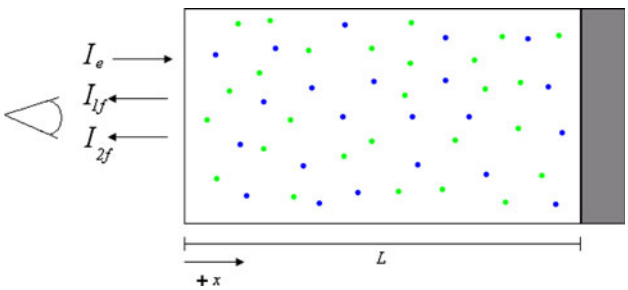

Fig. 2 Standard DELIF geometry for 2-dye system. The dyes responsible for the *high*-energy fluorescent emission and *lower* energy emission are represented by the *green* and *blue dots*

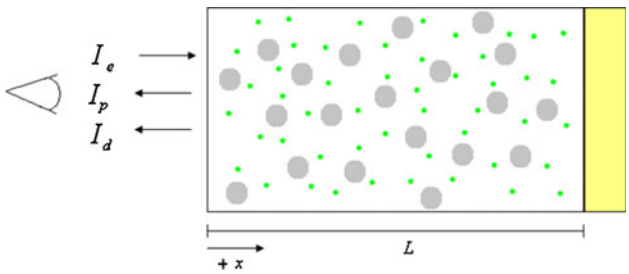

Fig. 3 Model system geometry. The high-energy-wavelength fluorophore is the pad. The reabsorbing fluorophore is the dye dissolved in the fluid (*green dots*). The fluid also contains large colloidal particles (*gray dots*) that scatter light

spectrum for Dye 2 overlaps the emission spectrum for Dye 1. The resulting fluorescent intensities of the two dyes exiting the fluid layer in the $-x$ direction are I_{f1} and I_{f2}. These two signals are acquired by the CCD elements in the cameras and are combined to produce the final DELIF image.

The DELIF geometry for a single-dye CMP setup is illustrated in Fig. 3. In this system, Dye 1 has been eliminated because it has a similar fluorescent spectrum to the polyurethane polishing pad located at $x = L$. The large particles in Fig. 3 represent the slurry particles, which are capable of scattering light. As the laser light travels through the fluid, it only excites Dye 2 until it reaches the pad, at which point the pad fluorescence begins to travel in the $-x$ direction where some of the fluorescence is reabsorbed by Dye 2. Inside the column of fluid, all signals can experience scattering, leading to a greater optical density in the fluid. A fraction of the fluorescence from the pad, I_p, and Dye 2, I_d, that exit the fluid layer in the $-x$ direction are collected by a lens in front of the two cameras. The two camera images can then be combined to create the ratiometric DELIF image using Eq. 1.

Propagation of light through a medium can be described by the radiative transfer equation:

$$\mathrm{d}I = (\sigma_{\mathrm{em}} - I\sigma_{\mathrm{ext}})\mathrm{d}x. \tag{2}$$

Equation 2 has a term representing the generation of new light, σ_{em}, and a term that represents the degradation of existing light, $-I\sigma_{\mathrm{ext}}$. Note that σ_{em} has the units of intensity, or radiant flux per unit distance because it represents the generation of light in a system, and σ_{ext} is a coefficient per unit distance that represents the fraction of existing radiant flux, I, lost in the system. The extinction coefficient, σ_{ext}, represents intensity losses from both light absorption, in accordance with Beer's Law, and scattering, in accordance with Rayleigh, Mie, or geometric scattering theories depending on scattering particle size (Chandrasekhar 1960). Assuming that each scattering particle has the same radial scattering distributions and that the particles are evenly dispersed throughout the slurry, we can consider a 1-dimensional ray propagation model with effective forward, μ_f, and backward, μ_b, scattering coefficients. If the particles are evenly dispersed, there is no need for a complex 3-dimensional model because lateral light scattering off a single particle will be canceled by a neighboring particle (Hecht 2002). Initially, it would seem that this assumption is valid, since the slurry film thickness is very thin compared to its width. However, local microscale pad topology exists on the same order as the fluid film thickness. Therefore, there are some valid concerns that the one-dimensional assumption may introduce some inaccuracies for CMP. Indeed, complex flow patterns around pad asperities could cause an uneven distribution of particles (Muldowney 2007). Nevertheless, the analytical simplicity of the one-dimensional model is sufficient to evaluate the qualitative effects of absorption, emission, and scattering variables within this system.

Figure 4 is a schematic framework for casting the system of transfer equations needed for modeling the DELIF system. The surface of the fluid is at position $x = 0$, and the surface of the pad is located at the position $x = L$. In reality, the pad surface is quite rough compared to the height of the column of fluid (Gray 2008). However, we will assume a flat pad for an infinitely narrow column of fluid for this 1-dimensional model. To complete the model, we consider an infinitely small segment of fluid within the column, dx, represented by the box in the middle of the column of fluid in Fig. 4. Across dx, light is scattered by the colloidal particles and absorbed and emitted by the dye dissolved in the fluid. It is necessary to consider light propagation in both the $+x$ and $-x$ directions because dye emission is induced by light traveling in either direction. We will also assume the fluorescence is an isotropic emission. The values of $I_d^-(x = 0)$ and $I_p^-(x = 0)$ are equivalent to I_{f1} and I_{f2}, respectively, in Eq. 1 and are used to create the DELIF image. They are visually represented by I_p and I_d in Fig. 3. These values are influenced by light traveling in both the $+x$ and $-x$ directions.

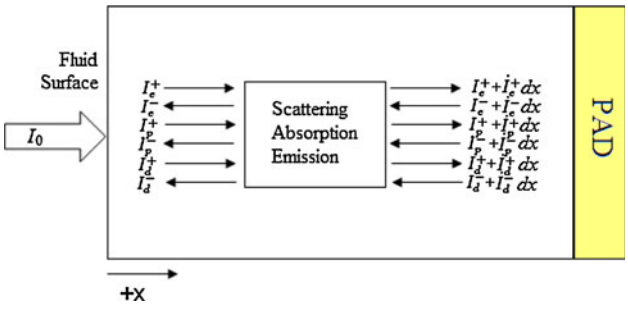

Fig. 4 Propagation directions of light through the fluid layer

There are three sources of light in our system: laser, dye, and pad. As Fig. 4 illustrates, these light sources travel in both the $+x$ and $-x$ direction. This yields a system of six linear, first order, ordinary differential equations (ODEs) that can be represented in matrix format shown in Eqs. 3 and 4.

$$\frac{\mathrm{d}\mathbf{I}}{\mathrm{d}x} = \mathbf{K} \cdot \mathbf{I} \tag{3}$$

$$\begin{bmatrix} I_e^+ \\ I_e^- \\ I_p^+ \\ I_p^- \\ I_d^+ \\ I_d^- \end{bmatrix} = \begin{bmatrix} -(k_1+k_3) & \mu_b C_{Si} & 0 & 0 & 0 & 0 \\ -\mu_b C_{Si} & k_1+k_3 & 0 & 0 & 0 & 0 \\ 0 & 0 & -(k_2+k_3) & \mu_b C_{Si} & 0 & 0 \\ 0 & 0 & -\mu_b C_{Si} & k_2+k_3 & 0 & 0 \\ k_1k_4 & k_1k_4 & k_2k_4 & k_2k_4 & -k_3 & \mu_b C_{Si} \\ -k_1k_4 & -k_1k_4 & -k_2k_4 & -k_2k_4 & -\mu_b C_{Si} & k_3 \end{bmatrix} \cdot \begin{bmatrix} I_e^+ \\ I_e^- \\ I_p^+ \\ I_p^- \\ I_d^+ \\ I_d^- \end{bmatrix} \tag{4}$$

Equation 4 is essentially Eq. 2, the radiative transfer equation, written for coupled intensity components. The constants in the **K** matrix represent intensity gains and losses due to all the other components in the CMP DELIF system. The elements of **K** can change with the assumptions made about the system. Since I_e and I_p are generated at the boundaries of the fluid layer and only degrade inside the fluid, these terms only contain extinction terms related to scattering, $\mu_b C_{Si}$ and k_3, and absorption, k_1 and k_2. The I_d term contains both σ_{em} and σ_{ext} terms because the dye emission is both generated within the film and scattered throughout. The σ_{em} term for I_d includes intensity generation due to the laser emission, $k_1k_4I_e$, and the pad emission, $k_2k_4I_p$. The σ_{ext} terms for I_d include k_3 and $\mu_b C_{Si}$. All of these terms will be defined further in the following text.

Constant, k_1, represents the absorption coefficient of the dye at the wavelength of the laser emission:

$$k_1 = \varepsilon_d(\lambda_l) C_d, \tag{5}$$

where $\varepsilon_d(\lambda_l)$ is the absorption coefficient at the wavelength of the laser, and C_d is the concentration of the dye.

Constant, k_2, represents the average spectral absorption of the dye and is expressed as an integral over all wavelengths of the pad emission:

$$k_2 = \frac{\int \varepsilon_d(\lambda_p) C_d d\lambda_p}{\bar{\lambda}_p}, \tag{6}$$

where $\varepsilon_d(\lambda_p)$ is the absorption coefficient at the wavelengths of the pad emission, and $\bar{\lambda}_p$ is the width of the spectral band of the absorption.

Light scattering within the fluid layer is captured in the terms $\mu_b C_{Si}$ and k_3, where k_3 is equal to:

$$k_3 = \mu_f C_{Si}, \tag{7}$$

and C_{Si} is a term that represents the concentration of the scattering particles. In many CMP slurries, these particles are often colloidal or fumed silica that have a relatively monodispersed size distribution. In this model, it is assumed that scattering due to slurry particles is the dominant term in the extinction coefficient. Additionally, absorption of light by the scattering particles is minimal or nonexistent. We are also assuming that the dye itself does not scatter light and the dye does not absorb its own emission. In reality, there is less than a 2% overlap in the absorption and emission spectra for Calcein dye, which has often been used in CMP DELIF systems (Gray 2005). The dye could potentially scatter light if it is not fully dissolved in the fluid. If we were to consider the effects of dye scattering, extinction terms would appear in the off-diagonal terms K_{12}, K_{21}, K_{34}, K_{43}, K_{56}, and K_{65}.

Constant k_4 represents the emission coefficient of the dye:

$$k_4 = \frac{\phi_d}{2\bar{\lambda}_d} \int \eta_d(\lambda_d) \mathrm{d}\lambda_d, , \tag{8}$$

where ϕ_d is the quantum efficiency of the dye and $\eta_d(\lambda_d)$ is the emission constant of the dye at wavelength, λ_d, and $\bar{\lambda}_d$ is the width of the spectral band of the emission.

All constants in the **K** matrix can be obtained experimentally. Experimental determination of these values will not be discussed in this article. In order to maintain generality of this model, all the constants will be normalized and the sensitivities will be evaluated by varying the values of all constants on a scale from 0 to 1.

The closed form solution to each of these six ODEs will have the form:

$$\mathbf{I}(x) = \sum_{n=1}^{6} A_n e^{\beta_n x} \tag{9}$$

The exponents, β_n, in Eq. 9 are the eigenvalues of the **K** matrix. The coefficients, A_n, are determined by applying the boundary conditions at $x = 0$ and $x = L$. These boundary conditions are listed in Eqs. 10–15. The excitation energy at the surface of the fluid is the same as the incident light intensity.

$$I_e^+(0) = I_0 \tag{10}$$

The excitation energy at the pad surface, $x = L$, is the amount of light that is not absorbed, but reflected off of the pad surface. The constant, k_6, is the fraction of laser light moving in the $+x$ direction that is reflected to the $-x$ direction.

$$I_e^-(L) = k_6 I_e^+(L) \tag{11}$$

Since the polishing pad only emits light at $x = L$, there is no pad light traveling in the $+x$ direction at the surface of the fluid ($x = 0$).

$$I_p^+(0) = 0 \tag{12}$$

At $x = L$, the pad produces a fluorescent signal as a result of the excitation light present at $x = L$. The constant, $k_5 = \alpha(\lambda_l)\phi_p\eta_p(\lambda_p)$, is representative of the fluorescence produced by the pad.

$$I_p^-(L) = k_5 I_e^+(L) \tag{13}$$

The dye only fluoresces inside the fluid layer, and the dye does not produce a fluorescence at the surface of the fluid ($x = 0$) in the $+x$ direction.

$$I_d^+(0) = 0 \tag{14}$$

A fraction of the dye light from the $+x$ direction, ρ, is reflected off the pad surface into the $-x$ direction.

$$I_d^-(L) = \rho I_d^+(L) \tag{15}$$

The full algebraic closed form solution to these equations with the given boundary conditions has been calculated but is extraordinarily lengthy and will not be presented here. We have made a few reasonable assumptions that reduce the number of ODEs from 6 to 4. These assumptions will be presented later in the text. The simplified version of this system of equations has solutions that are not as lengthy and proved to have characteristically similar results to the full model. Therefore, we can conclude that these simplified equations still yield representative intensity values and can be used to interpret the dominant features of the intensity components through the fluid layer.

The mean slurry particle size for a typical CMP slurry ranges from 80 to 100 nm, which results in Mie scattering though the fluid layer. For this size particle, scattering is relatively isotropic (Bohren and Huffman 1998), meaning $\mu_b C_{Si} \approx k_3 \approx \mu_f C_{Si}$. The mean free path of a single photon is on the order of 10^3 μm as estimated using Mie scattering theory (Bohren and Huffman 1998) for slurry with high particle loading. Since the single photon mean

free path is much larger than the fluid layer thicknesses interrogated, it may be reasonable to assume that the effects of scattering are small. In the following simplified model, we set the backward scattering coefficients to zero just to eliminate the off-diagonal terms and simplify the solution, but we still will examine the effect of changing the forward scattering coefficients. Note that the assumption $\mu_b \to 0$ is consistent with smaller scattering particles, approaching the Rayleigh scattering regime.

Assuming scattering effects are small, it can also be assumed that $I_p^+(x) = 0$. If the laser light in the $+x$ direction is nearly completely absorbed by the dye and at the pad surface $x = L$, then the fraction of the laser light reflected off the pad into the $-x$ direction is minimal. Therefore, it may be reasonable to assume that there is no laser light traveling in the $-x$ direction, $I_e^-(x) = 0$. This simplification also assumes the effects of scattering on the laser light are small. The assumptions that (1) scattering effects are small and (2) the majority of the incident laser light is absorbed through the fluid layer reduce the **K** matrix from a 6×6 to a 4×4 and eliminate some of the off-diagonal terms in the matrix. Additionally, boundary conditions 11 and 12 are eliminated because $I_e^-(x) = 0$ and $I_p^+(x) = 0$.

The simplified **K** matrix is shown in Eq. 16 and is based on the assumptions above. We did complete an analysis on the 6×6 **K** matrix, which includes both forward and backward scattering. However, the 6×6 **K** matrix equations proved to be a much more complex equation system and cumbersome to evaluate, while yielding similar intensity curves to those predicted by the 4×4 **K** matrix model. Therefore, we will focus our discussion on the solution to Eq. 16.

$$\begin{bmatrix} \dot{I}_e^+ \\ \dot{I}_p^- \\ \dot{I}_d^+ \\ \dot{I}_d^- \end{bmatrix} = \begin{bmatrix} -(k_1+k_3) & 0 & 0 & 0 \\ 0 & k_2+k_3 & 0 & 0 \\ k_4k_1 & k_4k_2 & -k_3 & 0 \\ -k_4k_1 & -k_4k_2 & 0 & k_3 \end{bmatrix} \cdot \begin{bmatrix} I_e^+ \\ I_p^- \\ I_d^+ \\ I_d^- \end{bmatrix} \tag{16}$$

The solution to Eq. 16 was obtained using Mathematica Software (by Wolfram).

$$I_e^+(x) = I_0 e^{-(k_1+k_3)x} \tag{17}$$

$$I_p^-(x) = k_5 I_0 e^{(k_2+k_3)x-(k_1+k_2+2k_3)L} \tag{18}$$

$$I_d^+(x) = \frac{k_4 I_0 e^{-k_2 t - k_3(L+x)}}{(k_2+2k_3)} \times [(k_2+2k_3)e^{(k_2+k_3)L}(e^{-k_1 x}-1) + k_2 k_5 e^{-(k_1+k_3)L}(1-e^{(k_2+2k_3)x})] \tag{19}$$

$$I_d^-(x) = k_4 I_0 \left[\frac{k_1 e^{-(k_1+k_3)x}}{(k_1+2k_3)} - k_5 e^{-(k_1+k_2+2k_3)L+(k_2+k_3)x} + e^{k_3(x-2L)}\left[\frac{\rho(k_2+2k_3-k_2k_5e^{-(k_1+k_2+2k_3)L})}{k_2+2k_3} + \frac{k_5(k_2+2k_3+\rho k_2)e^{-k_1 L}}{k_2+2k_3} - \frac{(k_1+\rho k_1+2\rho k_3)e^{-k_1 L}}{k_1+2k_3}\right]\right] \tag{20}$$

These equations are the intensity traces in both the $+x$ and $-x$ directions for the laser excitation light, the pad and dye emission light through a fluid layer. There are six parameters, k_1 to k_5 and ρ, which describe the optical properties of the fluid layer and pad in the system and influence the response. In addition, there is the critical parameter, L, the fluid depth. This is the property of the fluid layer that we eventually want to be able to measure by looking at the intensity of both pad-wavelength and dye-wavelength light returning out through the boundary at $x = 0$. That is, $I_p^-(x = 0)$ and $I_d^-(x = 0)$.

In practice, the six material property parameters, k_1 to k_5 and ρ, must be determined experimentally. The dye absorption terms, k_1 and k_2, can be measure with a UV–Vis spectrophotometer using a known depth of fluid and dye concentration in the absence of scattering particles to solve for $\varepsilon_d(\lambda)$ (Harris 1989). The scattering efficiency term, μ_f, in k_3 is a function of the actual cross section of the particle relative to the effective cross section at a particular wavelength. This effective cross section effectively blocks the transmission of light. Scattering efficiency can also be measured using a UV–Vis spectrophotometer in the absence of the fluorescent dye. If the scattering particles are not opaque to UV and visible light, this method will also detect losses through the fluid due to particle absorption (Cox et al. 2002). The quantum yield, ϕ, in k_4 and k_5 is the ratio the photons absorbed to the photons emitted. This can typically be determined using a fluorometer (Gaigalas and Wang 2008). For measuring the polishing pad quantum yield, the fluorometer can be coupled with an integrating sphere to reduce scattering noise due to surface texture (Gaigalas and Wang 2008). The wavelength-dependent emission efficiency, $\eta(\lambda)$, in both k_4 and k_5 can be determined using a fluorometer as well, varying the incident excitation wavelength. This same technique can be used to determine the wavelength-dependent absorbance, $\alpha(\lambda)$, in k_5. The reflectance efficiency at a particular wavelength for the polishing pad, $\rho(\lambda)$, can be measured using an integrating sphere by measuring the amount of incident light at a wavelength, (λ), that is not absorbed by the material, but is collected a detector.

In the following discussion, we will be examining the solutions to Eq. 16 as we vary the material proper parameters k_1 to k_5 and ρ. For simplicity, the discussion will limit these variables to values between 0 and 1. The reader should note that the values of k_1, k_2, and k_3 are concentration dependent in addition to being dependent on efficiency terms. Therefore, the maximum value of these terms can be greater than 1 if the concentration term is greater than 1. However, the k_4, k_5, and ρ terms are solely dependent on absorption, emission, and quantum efficiency terms. These terms should not exceed a value of 1.

3 Discussion

The intensity of each system component in Eq. 16 is illustrated in Fig. 5, which shows each component as it propagates through the slurry layer. The results of Eqs. 17–20 are nondimensionalized by dividing both sides of the equations by I_0 and plotting I/I_0 as a function of nondimensional depth into the fluid layer, x/L. To start the discussion about the independent effects of each constant, the values of k_1 through k_5 and ρ are set to 1, and k_3 is set to 0 in Fig. 5. In this scenario, varying these constants individually between 0 and 1 would cause the intensity to decay or grow by a factor of $e^{\pm 1}$ over the film thickness.

In order to choose the correct dye and concentration for the DELIF system for CMP, we can use this model to predict whether or not the intensities of the pad and the dye exiting the fluid layer will be sufficient to produce a measurable ratiometric DELIF image. In order to predict the dye concentration that will be needed, we need to determine the absorption, emission, and scattering constants as described earlier. The dye concentration, C_d, and particle loading in the slurry, C_{Si}, can be varied until $I_p^-(x=0)$ and $I_d^-(x=0)$ reach detectable values. Increasing the concentration of the dye will increase the values of k_1 and k_2. Variations in scattering particle loading will increase the value of k_3.

Figure 5 illustrates a system with scattering, where $k_3 = 1$. Figure 6 illustrates the same system with no scattering, $k_3 = 0$. The intensities of all components decrease when scattering particles are present in the fluid layer because scattering contributes to the extinction of intensity elements in Eq. 16.

The value, k_1, represents the amount of laser light absorbed by the dye. As k_1 decreases from 1 to 0, the amount of dye light exiting the fluid layer, $I_d^-(x=0)$, decreases by 75% in a system without scattering particles and only 27% in a system with 100% efficient scattering particles. The remaining emission intensity is due solely to the absorption and re-emission of the light produced by the polishing pad. The dye emission intensity is decreased in a system with scattering particles because the emissions become trapped within the fluid layer. The amount of pad light exiting the fluid layer, $I_p^-(x=0)$, increases by a factor

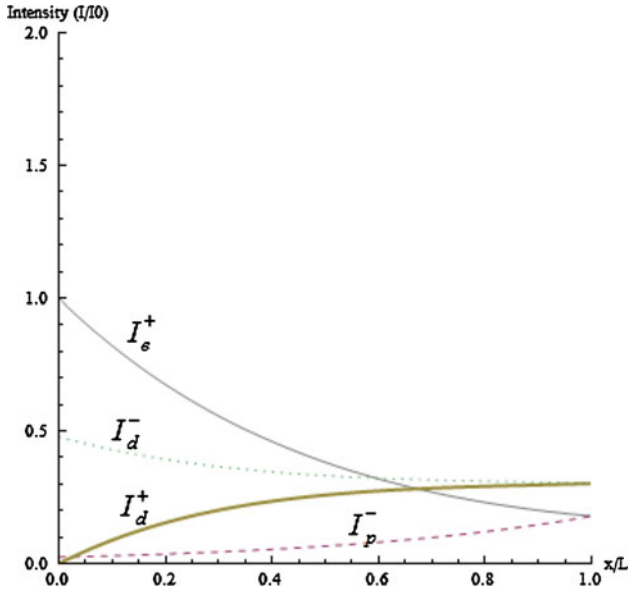

Fig. 5 Intensity of DELIF components through a column of fluid with scattering particles. I_e^+ is the intensity of the excitation energy in the $+x$ direction, I_p^- is the intensity of the polishing pad emission in the $-x$ direction, I_d^+ is the intensity of the dye emission in the $+x$ direction, and I_d^- is the intensity of the dye emission in the $-x$ direction

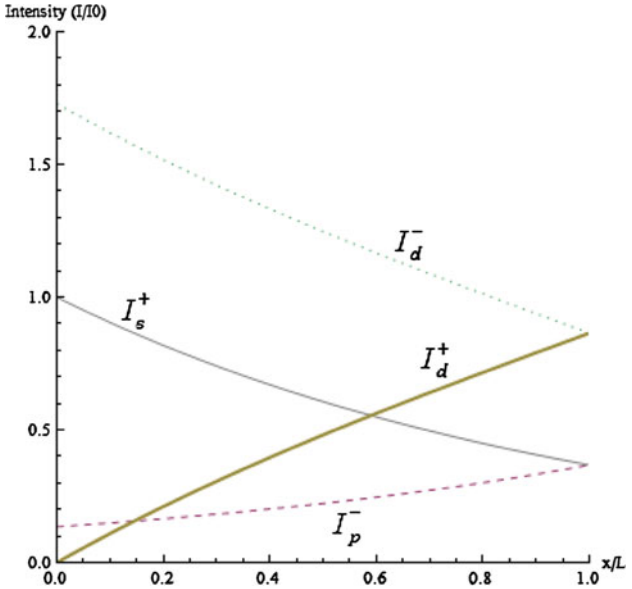

Fig. 6 Intensity of DELIF components through a column of fluid without forward scattering particles. I_e^+ is the intensity of the excitation energy in the $+x$ direction, I_p^- is the intensity of the polishing pad emission in the $-$x direction, I_d^+ is the intensity of the dye emission in the $+x$ direction, and I_d^- is the intensity of the dye emission in the $-x$ direction

of 170% as k_1 is decreased from 1 to 0. The percentage increase in pad emission intensity is independent of the value of k_3, the extinction due to scattering particles. This is because the dye absorption due to the pad emission, k_2, and the emission efficiency of the pad, k_5, is not affected by changes in k_1. Additionally, Eq. 16 does show that the pad emission intensity is not coupled to the dye emission.

The value, k_2, is representative of the efficiency of the dye absorption at the wavelength of the pad emission. When k_2 is decreased from 1 to 0, the dye intensity at the fluid surface, $I_d^-(x=0)$, decreases by 10% in a system with scattering particles, and 17% in a system without scattering particles. As k_2 is decreased from 1 to 0, the pad emission intensity, $I_p^-(x=0)$, increases by a factor of 170%, which is independent of the scattering term, k_3, also due to the fact that the pad emission is not coupled to the dye emission, as stated above. This model shows that the intensity of the dye emission exiting the fluid layer has a greater dependence on the ability of the dye to absorb the laser emission than the pad emission. This is because the intensity of the laser emission through the fluid layer is always greater than the intensity of the pad emission, illustrated in Figs. 5 and 6.

If the dye is incapable of absorbing the incident laser light, $k_1 = 0$, it can still absorb the emission of the pad provided that $k_2 \neq 0$. When $k_1 = 0$, the emission intensity of the dye is reduced by a factor of 27–75% depending on the degree of particle scattering in the system, $0 < k_3 < 1$. The percent decrease in intensity as $k_1 \to 0$ is less in system with higher k_3 values. This is probably a result of the scattering particles reflecting light back toward the dye molecules creating opportunities for further excitation within the fluid layer. Considering the opposite scenario where the dye is not absorbing any of the light from the laser and the pad is the only excitation source for the dye, $k_1 \neq 0$ and $k_2 \to 0$, the emission intensity of the dye exiting the fluid layer drops between 10% as k_2 is varied from 1 to 0, depending on the degree of scattering. This change has a less prominent effect because the fluorescent intensity of the pad only propagates in the $-x$ direction and will always have a lower intensity than the laser.

The fluorescent efficiency of the dye is represented by k_4, and the fluorescent efficiency of the pad is represented by k_5. In a typical DELIF system, the dye is a more efficient absorber at the wavelength of the higher energy fluorophore (in this case, the pad, I_p) than at the wavelength of the laser (I_e). However, the intensity of the laser emission, I_0, is usually greater than the fluorescence of the pad (which is stimulated by the laser). This implies that the intensity of the dye, $I_d(x)$, is a result of both the incident laser intensity and the pad emission. In the model, this can be seen by reducing the fluorescent efficiency of the pad, k_5, to 0 and observing that the intensity of the dye does not approach 0 ($I_d \neq 0$) and has significant value.

The constant, ρ, is representative of the amount of dye emission traveling in the forward direction, $+x$, which is reflected back toward the fluid surface in the $-x$ direction. If the pad is 100% efficient at reflecting the dye light ($\rho = 1$), then $I_d^+(L) = I_d^-(L)$ and these intensity traces intersect at $x = L$ as shown in Figs. 5 and 6. As ρ decreases, the initial intensity of the dye fluorescence at $x = L$ approaches zero and the intensity at the fluid surface $x = 0$ decreases. In a scattering system, where k_3 is large, the effect of decreasing ρ on the amount of dye light exiting the fluid layer in the $-x$ direction is minimized. Therefore, particle scattering serves to distribute the light within the fluid layer to produce more dye excitation, especially near the surface of the fluid.

A DELIF image is produced by dividing pixels in the image of the dye fluorescence by the pixels in an image of the reabsorbed fluorophore (the pad), at the surface of the fluid ($x = 0$). The intensities collected by the cameras in a DELIF system are reduced from the initial intensity values exiting the fluid layer, $I_d^-(x=0)$ and $I_p^-(x=0)$, due to the losses in the optical path between the fluid surface and camera. Assuming the optical path losses for the dye camera and the pad camera are similar, the DELIF ratiometric image used to determine fluid layer thickness, R, is expressed in Eq. 21.

$$R = \frac{I_d^-(x=0)}{I_p^-(x=0)} \tag{21}$$

Substituting Eqs. 18 and 20 into Eq. 21 yields:

$$R = \frac{k_4 e^{(k_1+k_2+2k_3)L}}{k_5} \times \left[\frac{k_1}{k_1+2k_3} - k_5 e^{-(k_1+k_2+2k_3)L} + \left(\frac{\rho(k_2+2k_3-k_2k_5 e^{-(k_1+k_2+2k_3)L})}{k_2+2k_3} + \frac{k_5(k_2+2k_3+\rho k_2)e^{-k_1 L}}{k_2+2k_3} - \frac{(k_1+\rho k_1+2\rho k_3)e^{-k_1 L}}{k_1+2k_3} \right) e^{-2k_3 L} \right] \tag{22}$$

Note that the effects of the incident light, I_0, cancel in this ratio, fulfilling an essential DELIF assumption; the final image is dependent only on the fluid thickness, L, and not the incident light. The fluorescent efficiency of the dye represented by k_4 and the fluorescent efficiency of the pad represented by k_5 must be non-zero. Therefore, all three components of the intensity, I_e, I_p and I_d, must not be extinguished too greatly over the depth of the film. Additionally, both the pad and the dye must absorb and reemit the light within the system. The reflectivity of the incident dye light of the pad, ρ, can take any value and does not affect the linearity of the final DELIF ratio.

Another important assumption for applying DELIF to the in situ CMP measurement environment is that the relationship between R and L becomes linear for small values of L. We can see that this is not the case for the system depicted in Fig. 3 and modeled in the equations above. Using the simplification, $e^u = u$ for small values of u, Eq. 22 simplifies to Eq. 23, which is a cubic relationship between R and L.

$$R = \frac{k_1 k_4 (k_1 + k_2 + 2k_3)}{k_5 (k_1 + 2k_3)} L + k_4 (k_1 + k_2 + 2k_3) (k_1 + k_2 + 2k_3 (1 - \rho / k_5)) L^2 + 2k_3 k_4 (k_1 + k_2 + 2k_3) \times \left[\frac{k_1 (k_1 + 2k_3 + \rho k_2) - \rho k_2 (k_1 + k_2 + 2k_3)}{k_2 + 2k_3} - \frac{k_1 + \rho (k_1 + 2k_3)}{k_5 (k_1 + 2k_3)} \right] L^3 \quad (23)$$

For small enough values of L, the quadratic and cubic terms in Eq. 23 would become insignificant. In this regime, the relationship between R and L would be linear.

Figure 7 shows the effect of scattering particles on the DELIF ratio, R, is shown through a fluid film thicknesses between $L = 0$ to an arbitrary normalized fluid layer thickness, $L = 1$. Here, we have set the constants, k_1, k_2, k_4, k_5 and ρ, equal to 1. The dashed line represents a system in which the scattering constant, k_3, has been set to 1, and the solid line represents a system where $k_3 = 0$. The inset graph in Fig. 7 shows the approximate linear regime for this system. For a given fluid depth, L, the intensity ratio is larger in a system with scattering particles than a system without scattering particles. Even though the intensity of both components, $I_d^-(0)$ and $I_p^-(0)$, decrease when scattering particles are present, the ratio of the intensities increases when scattering particles are present. This is because the pad intensity, $I_p^-(0)$, decreases more than the dye intensity, $I_d^-(0)$, decreases when scattering particles are present. Therefore, scattering particles could ultimately increase the contrast in a DELIF image.

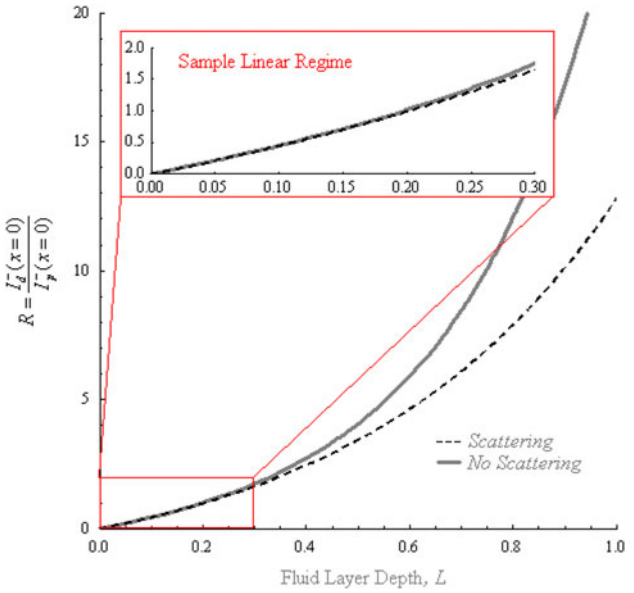

Fig. 7 The effect of scattering particles on the DELIF ratio. The inset graph shows the approximate linear region at small values of L

The curves in Fig. 7 eventually approach infinity at higher values of L. This is because the pad fluorescence is only located at the boundary $x = L$. $I_p^-(x)$, is the denominator of the ratio and approaches 0 as the fluid layer thickness increases. The vanishing of $I_p^-(x)$, is due to fluorescence reabsorption by the dye in the slurry. Scattering particles force the ratio to infinity faster because the optical density of the fluid is increased.

4 Experimental validation of model

The thickness of a thin fluid film between a polishing pad and a wafer on a table top CMP polisher was measured using a 2-camera, 1-dye DELIF system, which is thoroughly described elsewhere (Apone et al. 2005; Gray 2008), and briefly described here. We use Nd/YAG laser stepped to its second harmonic emission at 355 nm, with a power between 1.4 and 2.0 W. The beam is expanded and reflected toward a UV and optically transparent glass wafer coupled to the shaft on the table top polisher. The shaft is coupled to the glass wafer at the center of the wafer to allow us to image a large portion of the wafer. The laser emission stimulates the fluorescence of the polishing pad and the dye mixed into the slurry (Calcein) underneath the transparent wafer. These fluorescent emissions pass through the wafer and are reflected toward a magnification lens. The light passes through the lens toward a dichroic beam splitter that reflects wavelengths <475 nm to a camera at a 90° angle from the lens and transmits wavelengths >475 nm to the camera in line with the intake lens. The light traveling toward each camera is further filtered using band pass filters to isolate the peak emission wavelengths of the polishing pad (385–435 nm) and the dye in the slurry (540–570 nm).

It was necessary to use a custom manufactured "flat" polyurethane pad with a surface roughness (R_a) equal to 0.2 μm, during the calibration to minimize the noise from the surface roughness of the pad (compliments of Cabot Microelectronics). Flat polishing pads are not used in CMP because material removal and surface planarization of the substrate are dependent upon the ability of the pad asperities to transport the slurry particles to the surface being polished (Cook 1990). A typical R_a value for a commercially available polishing pad is between 4 and 20 μm (Nishioka et al. 1999). We have determined experimentally that the well depths must be at least five times the surface

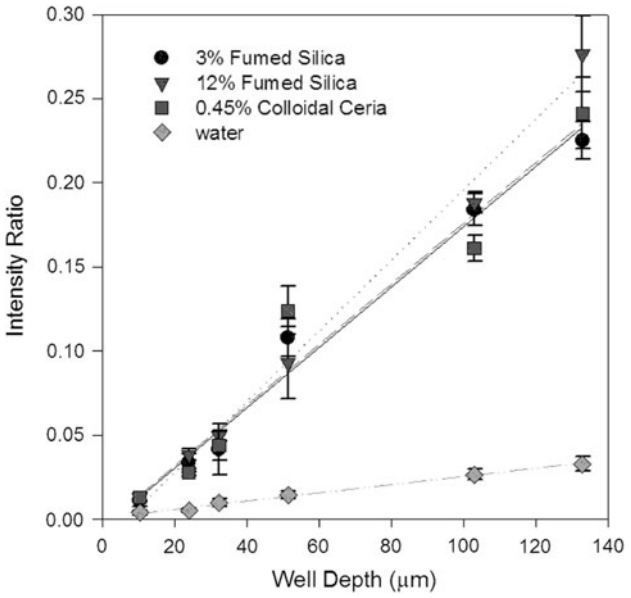

Fig. 8 The linear calibration of DELIF ratio intensity and well depth for four slurries with different scattering particle loading

roughness of the pad (Gray 2008). A discussion of how to calibrate using commercially available polishing pads is discussed elsewhere (Gray 2008).

Wells of different depths were etched into a Pyrex wafer such that we could measure a known thickness of fluid and calibrate the system. For a linear calibration, we need a minimum of two well depths, and for a quadratic calibration, we need at least three different well depths. To maximize the accuracy of our calibration and determine whether or not we were in a linear fluid depth regime, we chose to use six calibration wafers etched to the following depths: 10.3, 23.9, 32.3, 51.4, 103, and 133 μm. These calibration wafers were fixed to the table top CMP and DELIF setup described in the previous work (Coppeta and Rogers 1998; Chan 2003; Lu et al. 2000; Apone et al. 2005; Gray 2008). The effect of scattering coefficient of the 1-dye DELIF image ratio was studied by mixing Calcein dye at a concentration of 0.5 g/L, into 4 different slurries: water, 3% fumed silica, 12% fumed silica, and 0.45% colloidal ceria (all percentages are weight percent). For each slurry, scattering coefficients vary with wavelength (Garofalakis et al. 2004). We were able to perform a linear calibration for all four slurries as shown in Fig. 8. As predicted by our model, the slurry that produces the least intense DELIF ratio is the slurry without scattering particles. As the concentration of scattering particles increases, the DELIF ratio intensity increases, even though the intensity of the individual pad and dye images decrease. Therefore, the scattering particles produce a greater range of intensities over the well depths measured and produce a higher contrast resulting image.

The effects of scattering are greater at shorter wavelengths (Garofalakis et al. 2004). Therefore, scattering will decrease the intensity measured by the camera collecting the intensity of the polishing pad more than the intensity in the camera measuring the peak wavelengths of the Calcein dye emission. The reduced scattering coefficients, which are equivalent to the inverse of the mean free path of a photon within the media, are a function of the particle size, their scattering anisotropy, wavelength, and the particle concentration. Table 2 lists the calculated scattering coefficients for each of the measured slurries at the peak detection wavelengths for each camera, $\lambda = 410$ nm and $\lambda = 555$ nm. For this calculation, we assumed that all particles scatter light isotropically. The three slurries containing scatter particles have a calibration slope that is an order of magnitude larger than the calibration slope value for the dye water alone. The greatest slope value is for the slurry with the highest scattering coefficient, 22% silica. The 3% silica and 0.45% ceria slurries have similar scattering coefficients and have similar calibration slope values. This difference could be due to different particle refractive indices or the different geometries of the colloidal ceria versus fumed silica. Colloidal ceria particles are spherical and likely to scatter light isotropically, whereas fumed silica particles are likely to scatter light anisotropically because they are crystalline and irregularly shaped.

5 Conclusions and future work

We have created a new matrix-form optical model of the DELIF system for CMP based upon the radiative transfer equation. The model is for a 1-dimensional column of fluid in which absorption, emission, and scattering take place. We have also accounted for reflections and emissions from the polishing pad in our boundary conditions. Using this model, we can solve for the six equations representing the

Table 2 Summary of reduced scattering coefficients, calculated using Mie theory for each slurry type

Slurry type	Scattering coefficient (mm^{-1}) at $\lambda = 410$ nm	Scattering coefficient (mm^{-1}) at $\lambda = 555$ nm	Resulting calibration slope (nm^{-1})
12% Silica	8.66	4.79	2.10
3% Silica	2.17	1.20	1.79
0.45% Ceria	1.07	0.36	1.80
Water	0	0	0.24

intensities of the laser excitation source and the two fluorophores traveling in the $+x$ and $-x$ direction. The six resultant solutions can be quite complex but are similar in character to a simplified set of 4-equation. Solutions to the 4-equation model are presented for a DELIF system containing single dye dissolved in the fluid layer, accounting for a fluorescent polyurethane polishing pad at the fluid layer boundary, $x = L$. The resulting DELIF ratio, R, of the dye exiting the fluid, $I_d^-(x = 0)$, to the pad light exiting the fluid, $I_p^-(x = 0)$, for this single-dye system is shown to have a cubic dependence on the fluid depth, L. However, if the fluid layer is thin enough, the quadratic and cubic terms become negligible and the relationship between the DELIF image ratio intensity and the fluid thickness can be approximated as linear.

The effects of changing absorption and fluorescent efficiencies of the dye and the polishing pad were evaluated by varying the constants in the defining **K** matrix and boundary conditions. We have also evaluated the effects of scattering particles on this system because these particles are often found in CMP slurries. The six constants, k_1 to k_5 and ρ, were varied on a scale between 0 and 1. In reality, k_1, k_2, and k_3 are not limited to a maximum value of 1 because they contain dye and slurry particle concentration terms, which can exceed 1. However, k_4, k_5, and ρ should never exceed 1 because they only contain efficiency terms.

In order for DELIF to be a practical measurement technique for evaluating thin fluid films, the fluorescent efficiency of the polishing pad and the dye in the fluid layer must be non-zero. The absorption efficiency of the pad must also be non-zero, since it is considered in the denominator of the DELIF ratio. However, dye dissolved in the fluid layer is capable of absorbing the incident laser light and/or the emission of the pad. Therefore, measureable dye intensities can be made even in the absence of one of the fluorescent signals. Scattering particles increase the optical density of the fluid film and decrease the intensity of both the pad and the dye emission exiting the fluid layer by trapping the emissions within the fluid. While the intensity of the individual components of the DELIF ratio are decreased in a highly scattering system, the DELIF ratio itself increases when there are scattering particles present. This occurs because the pad fluorescence decreases more than the dye fluorescence.

We demonstrated experimentally that we can obtain a linear relationship between the DELIF ratio and the fluid thickness for small values of L, as demonstrated qualitatively by the model. This calibration is linear when the fluid depth is less than 133 um and up to 12 wt% fumed silica or 0.45 wt% colloidal ceria slurry. The experiment also evaluated increasing the concentration of scattering particles, which subsequently increases the intensity of the 1-dye DELIF system. In future work, we will report fluid depth data acquired on commercially available polishing pads. The system constants presented in the **K** matrix and the boundary conditions should be determined experimentally such that we can quantitatively evaluate the validity of this model against the experimental data.

Acknowledgments This project would not have been possible without the support of our funders: Intel Corporation, Cabot Microelectronics, and the NSF/SRC ERC with the University of Arizona. Many technical representatives from these organizations have provided input for this research. These representatives include Sriram Anjur from Cabot Microelectrons; Chris Barns formerly of Intel Corporation and presently from Cabot Microelectronics; Mansour Moinpour and Don Hooper from Intel Corporation; Professor Ara Philipossian from the University of Arizona; and Dr. Len Borucki, from Araca Corporation.

Appendix

By changing some of the constants in the defining 6×6 **K** matrix, we can also evaluate the system modeled by Coppeta and Rogers (1998) and Hidrovo and Hart (2001). The resulting DELIF ratio curve as a function of fluid layer thickness for the 2-dye system presented in previous literature is extraordinarily similar to the result to our equation presented below. This suggests that this model can be extended to consider a broad range of DELIF-type geometries.

In contrast to the 1-dye DELIF system, the DELIF ratio in a 2-dye system, shown in Fig. 2, never approaches infinity because both fluorophores are dispersed in the fluid and both fluorescent signals can reach the surface of the fluid at $x = 0$. The ratio in the 2-dye system actually asymptotes to a constant value as shown in Fig. 9. The matrix form of the radiative transfer equation used to calculate the curves in Fig. 8a is shown in Eq. 24.

$$\begin{bmatrix} \dot{I}_e^+ \\ \dot{I}_e^- \\ \dot{I}_p^+ \\ \dot{I}_p^- \\ \dot{I}_d^+ \\ \dot{I}_d^- \end{bmatrix} = \begin{bmatrix} -K_{1,1} & 0 & 0 & 0 & 0 & 0 \\ 0 & K_{1,1} & 0 & 0 & 0 & 0 \\ 0 & 0 & K_{3,3} & 0 & 0 & 0 \\ 0 & 0 & 0 & K_{3,3} & 0 & 0 \\ k_4(\lambda_l) & k_4(\lambda_l) & k_4(\lambda_p) & k_4(\lambda_p) & K_{5,5} & 0 \\ -k_4(\lambda_l) & -k_4(\lambda_l) & -k_4(\lambda_p) & -k_4(\lambda_p) & 0 & K_{5,5} \end{bmatrix} \cdot \begin{bmatrix} I_e^+ \\ I_e^- \\ I_p^+ \\ I_p^- \\ I_d^+ \\ I_d^- \end{bmatrix} \tag{24}$$

While the solutions for Eq. 24 used to calculate the ratio are more complex than the solutions achieved by Hidrovo and Hart (2001), the general shape of the curves from both models are very similar. In the 2-dye DELIF system, the depth of the fluid to which film thickness can be resolved appears deeper than the thickness indicated in the 1-dye system. However, these are qualitative results and the actual depths to which these systems can resolve film thickness need to be determined experimentally.

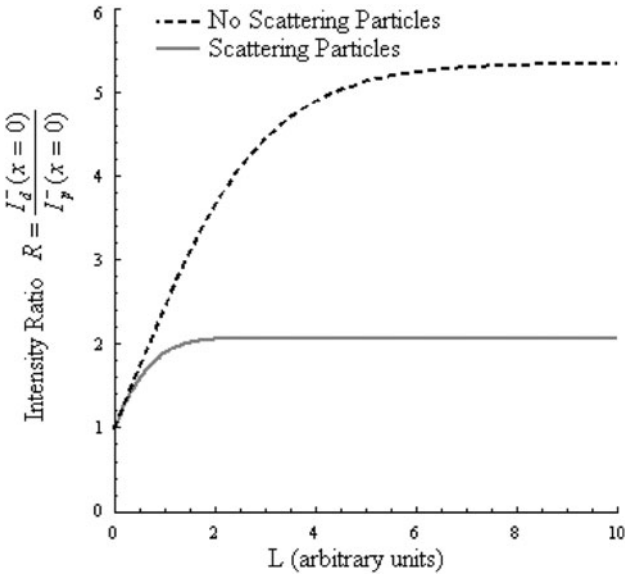

Fig. 9 Film thickness as a function of DELIF ratio using the matrix solution and showing the effects of scattering particles. This graph is very similar to the solution achieved by Hidrovo and Hart (2001)

The effect of adding scattering particles to the 2-dye DELIF system decreases the ratio value. Therefore, scattering particles have the opposite effect on the 2-dye than on the 1-dye system. In the 1-dye system, the decrease in ratio of dye intensities also corresponds to a decreased depth to which the ratio is an effective indicator of film thickness. The decrease in depth resolution will also produce decreased image contrast. In the 2-dye system, the increase in intensity due to the scattering particles increases image contrast. Provided that the observed pad fluorescence is significantly greater than the dark noise from the camera, image contrast and depth resolution should be increased by particle scattering in 1-dye DELIF.

References

Apone D, Gray C, Rogers C, Manno VP, Barns C, Moinpour M, Anjur S, Philipossian A (2005) Viewing asperity behavior under the wafer during CMP. Mater Res Soc Proc 867:W2.3.1–W2.3.7

Arcoumanis C, McGuirk JJ, Palma JMLM (1990) On the use of fluorescent dyes for concentration measurements in water flows. Exp Fluids 10:177–180

Bassnett S, Reinisch L, Beebe DC (1990) Intracellular pH measurement using single excitation-dual emission fluorescence ratios. Am J Physiol Cell Physiol 268(1):171–178

Bohren CF, Huffman DR (1998) Absorption and scattering of light by small particles. Wiley, New York

Chan EY (2003) Instantaneous mapping in chemical mechanical planarization. Master's thesis, Tufts University

Chandrasekhar S (1960) Radiative transfer. Dover Publications, New York

Cook LM (1990) Chemical processes in glass polishing. J Non-Cryst Solids 120:152–171

Coppeta J, Rogers C (1998) Dual emission laser induced fluorescence for direct planar scalar behavior measurements. Exp Fluids 26:1–15

Coppeta J, Rogers C, Philipossian A, Kaufman FB (1996) A technique for measuring slurry-flow dynamics during chemical-mechanical polishing. In: Materials research society proceedings, symposium L, fall

Coppeta J, Rogers C, Racz L, Philipossian A, Kaufman FB (2000) Investigating slurry transport beneath a wafer during chemical mechanical polishing process. J Electrochem Soc 147(5):1903–1909

Cox AJ, DeWeerd AJ, Linden J (2002) An experiment to measure Mie and Rayleigh total scattering cross sections. Am J Phys 70(6):620–625

Gaigalas AJ, Wang L (2008) Measurement of fluorescent quantum yield using a spectrometer with an integrating sphere detector. J Res Natl Inst Stand Technol 113(1):17–28

Garofalakis A, Zacharakis G, Filippidis G, Sanidas E, Tsiftsis D, Ntziachristos V, Papazoglou T, Ripoll J (2004) Characterization of the reduced scattering coefficient for optically thin samples: theory and experiments. J Opt A Pure Appl Opt 6:726–735

Gray C (2005) Measurement of pad compression during chemical mechanical polishing. Master's thesis, Tufts University

Gray C (2008) Detecting pad-wafer contact in CMP using dual emission laser induced fluorescence. Ph. D. Thesis, Tufts University

Gray C, Apone D, Rogers C, Manno VP, Barns C, Moinpour M, Anjur S, Philipossian A (2005) Viewing asperity behavior under the wafer during CMP. Electrochem Solid State Lett 8:G109–G111

Harris DC (1989) Symmetry and spectroscopy: an introduction to vibrational and electronic spectroscopy. Dover Publications, Mineola

Hecht E (2002) Optics 4th edn. Pearson Addison Wesley, San Francisco

Hidrovo CH, Hart DP (2001) Emission reabsorption laser induced fluorescence (ERLIF) film thickness measurement. Meas Sci Technol 12:467–477

Hidrovo CH, Brau RR, Hart DP (2004) Excitation nonlinearities in emission reabsorption laser-induced fluorescence. App Opt 43(4):894–913

Li Z, Lee H, Borucki L, Rogers C, Kikuma R, Rikita N, Nagasawa K, Philipossian A (2006) Effects of disk design and kinematics of conditioners on process hydrodynamics during copper CMP. J Electrochem Soc 153(5):G399–G404

Lu J, Coppeta J, Rogers C, Racz L, Philipossian A, Kaufman FB (2000) The effect of wafer shape on slurry film thickness and friction correlation in chemical mechanical planarization. Mater Res Soc Proc 613:E1.2

McQuarrie DA, Simon JD (1997) Physical chemistry: a molecular approach, chap. 15. University Science Books, p 626

Muldowney GP (2007) Advances in understanding and control of CMP performance: contact-hydrodynamics at wafer, groove and asperity scale. Mater Res Soc Symp Proc 991:153–164

Nishioka T, Sekine K, Tateyama Y (1999) Modeling on hydrodynamic effects of pad surface roughness in CMP process, interconnect technology 1999. In: IEEE international conference, pp 89–91, May 1999

Rogers C, Coppeta J, Racz L, Philipossian A, Kaufman FB, Bramono D (1998) Analysis of flow between a wafer and pad during CMP processes. J Electron Mater 27(10):1082–1087

Sakakibara J, Adrian RJ (1999) Whole field measurement of temperature in water using two-color laser induced fluorescence. Exp Fluids 26:7–15

Sakakibara J, Adrian RJ (2004) Measurement of temperature field of a rayleigh-benard convection using two-color laser-induced fluorescence. Exp Fluids 37:331–340

Shlien DJ (1998) Instantaneous concentration field measurement technique from flow visualization photographs. Exp Fluids 6:541–546

Strömberg N, Hulth S (2005) Assessing an imaging ammonium sensor using time correlated pixel-by-pixel calibration. Analytical Chemica Acta 550:61–68